

Shifted Helical CT to Optimize Cardiac PET-CT Co-Registration: Quantitative Improvement and Limitations

Journal:	<i>Molecular Imaging</i>
Manuscript ID:	MI-2009-09-0046.R1
Manuscript Type:	Research Articles
Keywords - General Terms:	cardiovascular, new PET/SPECT Instrumentation, novel imaging methods/agents for clinical studies
Keywords - Detailed Scientific Terms:	PET/CT, cardiac imaging, cardiology (clinical)



Review

TITLE: Shifted Helical CT to Optimize Cardiac PET-CT Co-Registration: Quantitative Improvement and Limitations

AUTHORS AND AFFILIATIONS:

1. Nils P. Johnson, M.D.¹
2. Tinsu Pan, Ph.D.²
3. K. Lance Gould, M.D.³

1. Division of Cardiology, Department of Medicine, Northwestern University Feinberg School of Medicine, Chicago, Illinois
2. Imaging Physics Department, M.D. Anderson Cancer Center, University of Texas, Houston, Texas
3. Weatherhead P.E.T. Center For Preventing and Reversing Atherosclerosis, Division of Cardiology, Department of Medicine, University of Texas Medical School and Memorial Hermann Hospital, Houston, Texas

CORRESPONDING AUTHOR CONTACT INFORMATION:

K. Lance Gould, M.D.
University of Texas Medical School
6431 Fannin St., Room 4.256 MSB
Houston, TX 77030
Phone: 713-500-6611
Fax: 713-500-6615
Email: K.Lance.Gould@uth.tmc.edu

RUNNING TITLE: Shifted Helical Cardiac PET-CT

KEYWORDS: PET/CT imaging; attenuation correction; image artifacts; myocardial perfusion; PET instrumentation

ABSTRACT

Combined computed tomography (CT)-positron emission tomography (PET) scanners utilize CT attenuation correction but suffer from misregistration artifacts. However, the quantitative accuracy of helical versus cine CT in the same patient after optimized co-registration by shifting both CT data as needed for each patient is not known. We studied 293 consecutive patients undergoing cardiac perfusion PET-CT using helical CT attenuation correction for comparison to cine CT. Objective, quantitative criteria identified PET-CT misregistration and associated perfusion abnormalities. Custom software shifted CT data to optimize co-registration with quantitative artifact improvement. The majority (58.1%) of cases with both helical CT and shifted helical CT data (N=93) had artifacts that improved or resolved by software shifting helical CT data. Translation of shifted helical CT was greatest in the x-direction (8.8 ± 3.3 mm) and less in the y- and z-directions (approximately 3.5 mm). The magnitude of differences in quantitative endpoints was greatest for helical CT ($P=0.0001$, N=177 studies), less for shifted helical CT but significant ($P=0.0001$, N=93 studies), and least for cine CT (NS, N=161 studies) compared to optimal attenuation correction for each patient. Frequent artifacts due to attenuation-emission misregistration are substantially corrected by software shifting helical CT scans to achieve proper co-registration that, however, remains on average significantly inferior to cine CT attenuation quantitatively.

Deleted: of cases

INTRODUCTION

Cardiac positron emission tomography (PET) offers the most accurate quantitative noninvasive assessment of myocardial perfusion (1). A key component of its accuracy rests with attenuation correction. Traditionally a rotating rod source has been used to generate a transmission image. However combined computed tomography (CT)-PET technology now provides CT attenuation maps. Current guidelines make no explicit mention of recommended CT attenuation technique (2,3) or offer broad suggestions of a 10-60 second CT scan during free breathing (4) in view of the optimal approach still being debated. Several groups have demonstrated frequent artifacts in cardiac PET-CT due to both misalignment and respiration occurring with both fast and slow CT acquisitions, with proposed solutions (5-14). Prior work from our group has demonstrated the extent, clinical significance, and implications of such artifacts (15) with validated solutions using either pre-rest and post-stress cine CT (10) or a single post-stress cine CT to reduce radiation dose (16). However, neither our prior work (10, 16) nor the existing literature quantitatively compares helical CT PET and cine CT PET images, both with optimized co-registration by shifting CT data as needed.

Thus, no literature to-date has compared helical versus cine CT in the same patient after each attenuation CT map has been optimally shifted. Such a comparison is important since some PET-CT scanners do not have cine CT capability. Therefore, we explored the quantitative accuracy, clinical benefits and limitations of using software-shifted helical CT attenuation correction as an alternative that is more widely available than cine CT attenuation correction in cardiac PET.

MATERIAL AND METHODS

Study Patients

We studied 293 consecutive patients undergoing diagnostic myocardial perfusion rest-dipyridamole PET-CT for potential coronary artery disease (CAD) evaluation or follow-up imaging at the Weatherhead PET Center for Preventing and Reversing Atherosclerosis of the University of Texas Medical School-Houston and Memorial Hermann Hospital. All subjects signed a clinical informed consent approved by the Committee for the Protection of Human Subjects of the University of Texas Health Science Center.

PET Acquisition Protocol

Patients were instructed to fast for 4 hours and abstain from caffeine, theophylline, and cigarettes for 24 hours before the study. PET-CT was performed using a Discovery ST 16-slice PET-CT multislice bismuth germanate tomograph (GE Healthcare) in two-dimensional mode with extended septa at a reconstructed inplane resolution of 5.9 mm full width at half maximum (FWHM). Patients were positioned in the scanner using laser guides aligned to the base of the throat and confirmed by a CT scout scan. External body markers were used to ensure correct positioning throughout data acquisition. Emission images were obtained over 6 minutes after intravenous injection of 1,295–1,850 MBq (35–50 mCi) of generator-produced ^{82}Rb and contained 24–60 million total counts, of which 12–30 million were true coincidence counts. Selected patients with severe unresolved complex attenuation issues on shifted helical or cine CT-PET scans were restudied on a Positron Corporation PET scanner with rotating rod attenuation acquisition and correction using the same rest-stress and imaging protocol and same doses of ^{82}Rb .

Immediately after completing the resting ^{82}Rb scan, dipyridamole (0.142 mg/kg/min) was infused for 4 minutes. Four minutes after completion of the dipyridamole infusion, the same dose of ^{82}Rb was given intravenously. Emission image acquisition was started at 70 seconds (or 80 seconds for patients

with heart failure or heart rates below 55 beats per minute) after the beginning of ^{82}Rb infusion. For dipyridamole-induced angina, aminophylline (125 mg) was given intravenously. All protocols, data acquisition, processing and quantification of cardiac PET and PET-CT are as previously reported (10, 15-19).

CT Acquisition Protocol

Helical and cine CT scans were performed both before rest emission imaging and after stress emission imaging. All patients were imaged using helical CT attenuation correction. Helical CT transmission scans were obtained at 120 kV and 100 mA over 29 seconds during normal breathing (in a subset of patients) or over 4 seconds at end-expiratory breath-hold (in another subset of patients), as we compared slow versus fast methods of helical CT acquisition to minimize artifacts. The helical CT acquisition used x-ray collimation of 16 by 1.25 mm, gantry rotation of 0.5 seconds, and helical pitch of 1.75:1. The radiation exposure was 5.7 mGy for the helical CT scan.

A majority subset of patients was also imaged using cine CT attenuation correction as previously described (10). Cine-mode data acquisition is one of the 3 optional data acquisitions on the Discovery PET-CT scanner that include axial, helical, and cine modes. The cine CT scan used 120 kV, x-ray collimation of 8 by 2.5 mm, gantry rotation cycle of 0.5 seconds, cine duration of 10 seconds, and 14 cm coverage. Each reconstruction used 360° of CT data over 0.5 seconds. The cine data acquisition lasted for 78 seconds, of which 70 seconds was for 7 cine CT acquisitions of 10 seconds each and 8 seconds was for 6 table translations of 2 cm each between 2 cine CT acquisitions.

Tube current for cine CT was 10 mA for patients weighing <100 kg, 15 mA for 100–130 kg, and 20 mA for >130 kg (lower dose than standard helical protocol). The radiation dose and effective dose equivalent for cine CT were 10 mGy and 2.36 mSv, respectively, for a tube current of 10 mA. For each cine CT scan, there are 1,232 CT images reconstructed 2 min after the cine CT acquisition and 22 images per slice location during normal respiration before averaging into a composite CT image over

several breathing cycles. Interpolation of the average CT attenuation data was performed to make the average CT images align at the locations of the PET slices for attenuation correction.

In view of the inherent blurring introduced by the average CT but not by the helical CT data, we applied 4- and 10-mm FWHM Gaussian filtering on the average CT and helical CT data, respectively, before CT attenuation correction.

Image Reconstruction

Custom software was developed to shift the CT data if needed in horizontal and vertical directions in the transaxial plane and in the superior–inferior or z-axis direction of different planes to align the CT heart borders visually with the PET data to achieve good co-registration. Images were reconstructed using filtered backprojection with a Butterworth filter having a cutoff of 0.55, roll-off of 10, and pixel size of 3.27×3.27 mm. Fusion images were made by superimposing attenuation-corrected emission and CT transmission scans in horizontal, coronal, and sagittal views and shifted as needed to achieve optimal attenuation-emission coregistration.

After attenuation correction, the reconstructed PET emission images in DICOM format were exported to an Ultra 60 workstation (Sun Microsystems) of an mPower-HZL PET scanner (Positron Corporation) for reorientation into long- and short-axis tomographic and topographic three-dimensional displays using previously described automated quantitative software (17, 19-22). Quantitative data from ^{82}Rb and ^{18}F phantoms imaged on the Discovery ST scanner have been exported to the mPower-HZL software for automated quantitative analysis and the quantitative accuracy of exported data has been validated by extensive phantom studies.

A three-dimensional restructuring algorithm generates true short- and long-axis views from reconstructed PET transaxial cardiac images, perpendicular and parallel to the long axis of the left ventricle. From the tomographic data, circumferential profiles are used to reconstruct three-dimensional topographic views of the left ventricle showing relative regional activity distribution divided into lateral,

inferior, septal, and anterior quadrant views of the three-dimensional topographic display corresponding to the coronary arteries as previously described (17, 19-22) and illustrated in Figure 1.

Quantitative PET Image Analysis

Mean activity in each quadrant is normalized to the maximum 2% of pixels in the whole heart dataset. Regions of each quadrant are identified having values outside 2.0 and 2.5 standard deviation (SD) reference values of 50 healthy volunteers with no risk factors by complete medical history (no hypercholesterolemia, hypertension, diabetes, smoking, obesity, drug or alcohol abuse, other systemic diseases, or family history of CAD). The percentage of circumferential profile outside 2.0 and 2.5 SD was calculated automatically for each quadrant and the whole heart.

Deleted: units

The severity of a perfusion defect is quantified as the average relative uptake in a defined quadrant or the lowest quadrant average relative activity, i.e., the average relative activity for the quadrant having the lowest average activity of anterior, septal, lateral, and inferior quadrants for each subject, expressed as a percent of the highest 2% of activity in the image dataset. The highest quadrant average relative activity quantifies perfusion in the most normal quadrant for each subject. The size of perfusion defects is quantified as the fraction of the whole cardiac image outside 2.0 and 2.5 SD of controls in each quadrant and whole heart. The combined size and severity of perfusion defects are defined as the percent of the whole cardiac image with relative activity of less than 60% of maximum activity (100%), which is 3.0 SD below the mean maximum activity of controls. The percent of the whole cardiac image with relative activity of greater than 80% of maximum activity quantifies the normal area taking both size and severity into account. For a subset of patients done after our initial series studying PET-CT misregistration, absolute activity recovered by the scanner was computed by converting the raw counts to activity in $\mu\text{Ci/cc}$ using a linear calibrated conversion formula in automated software for the subgroups of patients processed after quantitative GE-to-Positron had been validated by phantom experiments.

Deleted: A

Taking the pixel-by-pixel ratio of the stress and rest images defines a stress/rest image. This can be done after both rest and stress scan have either been scaled by their respective maximums (so-called

relative stress/rest image) or converted to absolute activity via the linear calibration conversion formula (absolute stress/rest image). Histogram profiles of these stress/rest images are computed to quantify the percentage of the image with low (≤ 0.66 relative, ≤ 0.90 absolute), borderline (0.67-1.0 relative, 0.91-1.40 absolute), and normal (> 1.0 relative, > 1.40 absolute) values.

Misregistration Artifacts

On PET perfusion images, artifactual abnormalities due to misregistration were objectively defined as criteria (i) plus (ii), (iii), or (iv) as follows.

(i) The defect on the PET image was associated with a corresponding area of misregistration on the superimposed CT transmission and PET emission fusion scans.

(ii) An abnormality on the resting CT PET scan associated with misregistration disappeared, and the image normalized with correct co-registration of CT and PET emission data on the stress PET scan.

(iii) The abnormalities on the helical CT PET scan at rest or stress disappeared, and the image normalized with correct co-registration of CT and PET emission data on the cine CT PET scan or when the misregistration was corrected by shifting the cine CT scan to co-register visually with the PET scan.

(iv) The abnormality on helical CT PET disappeared on an additional separate rest–stress study repeated on the next day using an mPower-HZL standard PET scanner with a rotating rod transmission source and shift software to ensure correct registration of emission and transmission data as previously documented (15).

Therefore, to be counted as having an abnormality due to PET-CT misregistration, every patient with abnormal helical CT PET at rest or stress had to have a stress perfusion study with no significant regional defect after correct PET-CT co-registration. Any patient with a defect that persisted on stress PET-CT images or after correct co-registration that was outside 2 SD of healthy subjects was classified

as having a “real” defect, not an artifact, even if the defect improved after correct registration. Therefore, our observed prevalence of abnormalities due to PET-CT misregistration is a conservative underestimate.

For PET scans meeting the above criteria for misregistration artifacts, the severity, size, and combined size–severity of perfusion abnormalities in the same quadrant as the PET-CT misregistration were objectively quantified by automated software. Additionally, the perfusion abnormalities due to PET-CT misregistration with helical CT were visually graded after application of a shifted CT. This visual analysis was secondary to the quantitative endpoints, but performed to ensure the visual relevance of the findings and confirm the objective quantitative results as clinically consistent. The degree of improvement was graded as: no change, mild improvement, marked improvement, resolution, or worsening. The optimal amount of shift in each direction was recorded in mm when the shifted helical CT produced a superior image compared to helical CT. In addition to automated quantification of abnormalities, each PET study was visually interpreted for which method of CT attenuation produced the least artifact. This optimal set of images was deemed the gold standard for quantitative endpoints.

Statistical Methods

All statistical tests were performed using STATA version 10.1 (StataCorp, College Station, Texas). Continuous variables are expressed as mean \pm SD and were compared using the paired t-test. Proportions were compared using the chi-square or Fisher exact test. Differences from the gold standard were summarized using the quadratic mean and are expressed as mean (95% confidence interval). All applicable tests were two-tailed, and a $p < 0.05$ was taken as the cutoff for statistical significance.

Deleted: Kappa statistics were used to assess interobserver agreement.

RESULTS

We identified 293 consecutive patients who underwent PET-CT with data available for analysis, all of whom had helical CT scans for attenuation correction. In 161 cases (55.0%), a cine CT attenuation scan was also acquired. All CT attenuation maps (helical and/or cine) could be shifted if needed using custom software as detailed above to optimize co-registration. The 132 helical CT PET cases without cine CT served to contribute additional statistical power to the prevalence of misregistration artifacts that resolved after shifting helical CT data to achieve optimal co-registration. The quantitative comparison of helical CT-PET and cine CT-PET was analyzed in the 161 cases having CT data sets, both with optimized co-registration by shifting CT data as needed for each case.

Defect location and improvement

A total of 159 defects due to misregistration were identified on studies with helical CT attenuation. These were located in the lateral (N=66, 41.5%), anterior (N=50, 31.4%), inferior (N=36, 22.6%), and apical (N=7, 4.4%) regions of the left ventricle, totaling 100% of left ventricular regions. Those artifactual defects with at least a mild improvement after shifting the CT data were commonly located in the lateral (N=20, 30.3%), anterior (N=21, 42.0%), or apical (N=2, 28.6%) regions and less commonly in the inferior wall (N=4, 11.1%), totaling 100% of left ventricular regions. Thus, inferior misregistration artifacts were less likely corrected by shifting helical CT data compared to other regions.

A total of 78 defects due to misregistration were identified on studies with cine CT attenuation. These were located in the lateral (N=21, 26.9%), anterior (N=18, 23.1%), inferior (N=33, 42.3%), and apical (N=6, 7.7%) regions of the left ventricle, totaling 100% of LV regions. Again, those artifactual defects with at least a mild improvement were commonly located in the lateral (N=7, 33.3%) or anterior (N=6, 33.3%) walls and less commonly improved by shifting the cine CT data in the inferior (N=3, 9.1%) and apical (N=1, 16.7%) regions, totaling 100% of LV regions.

Helical Versus Shifted Helical CT

Tables 1 and 2 compare [relative myocardial uptake using](#) attenuation correction [by](#) helical CT with shifted helical CT in 93 patients (paired studies on the same patient using 2 different CT attenuation techniques). [Only a subset had absolute activity data \(N=13 rest, N=8 stress\) in addition to quantitative relative activity.](#) Figure 2 illustrates a severe artifactual defect due to attenuation-emission misregistration, corrected by shifting the helical CT data to co-register CT-emission scans on the fusion image. Both rest and stress artifacts are included in Table 1, while Table 2 distinguishes between artifacts observed on the rest image (N=66, 71.0%) and on the stress image (N=27, 29.0%). Both tables demonstrate that shifted helical CT attenuation reduces artifactually abnormal endpoints compared to helical CT attenuation, due to better co-registration on the shifted CT-PET images using shifted helical CT.

Deleted: using

[The change in visual assessment comparing shifted helical CT to helical CT attenuation](#) correction was scored for each study. The results were: no change (N=33, 35.5%), mild improvement (N=34, 36.6%), marked improvement (N=19, 20.4%), resolution (N=1, 1.1%), and worsening (N=6, 6.5%). The majority of cases (N=54, 58.1%) had artifacts that improved or resolved by using software-shifted helical CT instead of helical CT. A small minority (N=6, 6.5%) of cases had worsening artifacts using shifted CT attenuation data, when compared to perfusion assessed using unshifted cine CT attenuation data or on a stress study with improved co-registration or with a rotating-rod attenuation scan performed later, as detailed in the methods section.

Deleted: Table 3 compares binary cutoffs for abnormality in several endpoints using kappa statistics to assess interobserver agreement. All kappa p values achieve statistical significance, supporting the conclusion that helical CT and shifted helical CT do not agree on binary classification of abnormal scans, where shifted helical CT-PET has significantly fewer artifactual abnormalities than standard CT-PET.¶

The absolute spatial translation applied to create the shifted helical CT in each spatial dimension was quantified for each study. The average absolute x-axis shift was 8.8 ± 3.3 mm, y-axis shift was 3.5 ± 3.4 mm, and z-axis shift was 3.3 ± 5.5 mm. The x-direction required the greatest amount of shift, while the y- and z-directions had similar shift magnitudes. [Due to the slanted left heart border, vertical respiratory motion may cause lateral PET-CT misregistration in the x-axis.](#)

Helical Versus Cine CT

Tables 3 and 4 compare [relative myocardial uptake using attenuation correction by helical CT](#) with cine CT in 161 patients (paired studies on the same patient using 2 different CT attenuation techniques). [Only a subset studied after our initial analysis of misregistration had absolute activity data \(N=51 rest, N=16 stress\)](#). Figure 3 illustrates an artifactual defect due to attenuation-emission misregistration that was not corrected by software-shifting the helical CT but was corrected by cine CT data. Both rest and stress artifacts are included in Table 3, while Table 4 distinguishes between artifacts observed on the rest image (N=101, 62.7%) and on the stress image (N=60, 37.3%). Both tables demonstrate that cine CT attenuation reduces artifactually abnormal endpoints compared to helical CT attenuation, due to better co-registration on the cine CT-PET images.

Deleted: 4

Deleted: 5

Deleted: using

Deleted: 4

Deleted: 5

Comparison with Optimal CT Attenuation

In our data, cine CT was identified as the best attenuation scan with the least artifacts in the majority of cases (N=136, 76.8%) while in a minority of cases helical CT (N=31, 17.5%) and shifted helical CT (N=10, 5.6%) were judged to be the better or best attenuation image obtained.

Deleted: Table 6 compares binary cutoffs for abnormality in several endpoints using kappa statistics to assess interobserver agreement. All kappa p values achieve statistical significance, supporting the conclusion that helical CT and cine CT do not agree on binary classification of abnormal scans, where cine CT-PET has significantly fewer artifactual abnormalities than helical CT-PET.¶

Table 5 compares [both relative and absolute uptake](#) differences in quantitative endpoints between each type of attenuation scan and the optimal CT attenuation scan that may have been achieved by shifting either the helical or cine CT data or both. [Absolute activity data was only available for a subset \(N=67 helical, N=21 shifted helical, and N=67 cine\)](#). While many endpoints differ in absolute terms, the magnitude of difference is greatest for helical CT, less for shifted helical CT, and least for cine CT compared to whichever type of attenuation was judged optimal for each patient. Endpoints related to defect size and severity were most affected. For example, the percent of the scan below 60% of the maximum compared to using optimal CT attenuation differed by an absolute average of 7.5% (relative difference of 2.1) for helical-corrected studies, by an absolute average of 3.7% (relative difference of 1.5) for shifted helical-corrected studies, and by an absolute average of 0.7% (relative difference of 0.2) for cine-corrected studies, which were statistically significant. The percent of the scan outside 2.5SD compared to using optimal CT attenuation differed by an absolute average of 13.2% (relative difference of 1.8) for helical-corrected studies, by an absolute average of 9.3% (relative difference of 0.9) for shifted

Deleted: 7

helical-corrected studies, and by an absolute average of 1.6% (relative difference of 0.1) for cine-corrected studies, which were statistically significant.

Cine CT-PET has the least artifacts on average compared to helical or shifted helical CT-PET due to cine-CT most closely matching the average attenuation during breathing while acquiring the emission scan. However, a “big sigh” breath during cine CT may cause significant artifact, illustrated in Figure 4, not seen on helical CT-PET. Since it is easily recognized, the “big sigh” breath cycle can be removed from the CT attenuation data, using the remaining CT data during the remaining breathing cycles for attenuation correction, also shown in Figure 4.

Some attenuation artifacts on PET-CT cannot be corrected by shifting helical CT or by cine CT. Figure 5 illustrates a patient with an implanted defibrillator where the defibrillator cable in the right ventricle caused a high-density star artifact on the CT scan that over corrects the inferior region of the emission scan. This over correction of the inferior region caused relative severe anterior and lateral defect despite correct co-registration. In this case, repeat PET imaging using a Positron scanner with a rotating rod attenuation correction eliminated the artifactual anterior and lateral defects, as shown in Figure 5.

DISCUSSION

Our results support the use of software-shifted helical CT attenuation correction in cardiac PET-CT to minimize artifacts due to transmission/emission misregistration on a case-by-case basis. Both qualitative and quantitative data demonstrate improvement with decreased frequency and severity of artifacts after software shifting of helical CT-PET compared to helical CT PET images in the same patient with attenuation-emission misregistration.

Shifted helical CT attenuation correction improves on simple helical CT sufficient for most visual clinical interpretation. However, it does not achieve as much artifact suppression as cine CT, as shown by Tables 3-5 and prior work from our group (10). In Table 5, absolute activity recovery in using optimized helical CT attenuation correction is significantly different from cine CT that on average most closely matches the average attenuation during breathing while emission data is acquired. For quantifying absolute perfusion in cc/min/g (23) accurately, recovering absolute activity becomes crucial since flow models for determining perfusion in cc/min/g markedly enhance small differences in radionuclide uptake that are magnified into large differences in absolute flow.

Deleted: 4

Deleted: 7

Deleted: 7

For cardiac PET, each CT attenuation correction technique has a different propensity to produce artifacts, the greatest with helical CT, next shifted helical CT, next cine CT and least PET with rotating rod attenuation. Since PET-CT scanners were designed initially for cancer, brain or body imaging, these misregistration problems are greater for cardiac imaging that requires different, more complex technical hardware, software and protocols. Theoretically, classical cardiac PET with a three rod rotating attenuation correction method would have the least artifacts and therefore the best quantification with the lowest radiation exposure and comparable throughput capacity as PET-CT. However, our group has demonstrated that even rotating rod PET attenuation correction can create co-registration problems (15) and its unsupervised application will not produce consistently optimal results.

Our series of reports on cardiac PET-CT (10, 15, 16) emphasize those technical aspects required for definitive, stand alone, quantitative physiologic cardiac PET imaging as the basis for clinical decisions

and management not possible using any other technology (1, 17-22). To achieve this goal, our laboratory's current protocol consists of a low-dose resting helical CT scan during a breath hold, resting emission scan, stress emission scan and finally a cine CT scan while breathing. Images are routinely reconstructed with cine CT attenuation, checked for misregistration and software-shifted or the helical or software-shifted helical CT attenuation data used as needed.

Limitations of the Study

Formatted

Most current commercial PET-CT scanners lack appropriate hardware or software for cine CT. Some have cine CT capacity but average the cine CT data with the helical CT data that biases the cine CT data and lack the capacity for fusion images using the averaged cine-helical CT-PET data for visually assessing and correcting misregistration.

There are significant trade offs in dose and resolution between images optimized for cardiac versus extra-cardiac structures. In view of the higher radiation dose required for high quality CT imaging of extra-cardiac structures, it is reasonable to use lower CT dose for PET adequate for attenuation correction without formal interpretation of extra-cardiac structures that are sub-optimally imaged on attenuation scans.

Conclusions

Frequent artifacts due to attenuation-emission misregistration are substantially corrected in a specific patient by shifting the helical CT scans on attenuation-emission fusion images to achieve proper co-registration using custom software. However, helical CT attenuation correction either with or without shifting remains on average significantly inferior to cine CT attenuation on both qualitative and quantitative comparison. Since either helical or cine CT attenuation correction may be suboptimal in any individual patient, cardiac PET-CT for reliable, definitive, quantitative myocardial perfusion as an independent reliable guide to clinical management would optimally have the capacity for both helical and cine CT with software for shifting CT attenuation data to optimize co-registration with emission images as

needed for both helical and cine CT-PET protocols.

For Peer Review

REFERENCES

1. Gould KL. Positron emission tomography in coronary artery disease. *Curr Opin Cardiol* 2007;22:422-8.
2. Hesse B, Tägil K, Cuocolo A, et al; EANM/ESC Group. EANM/ESC procedural guidelines for myocardial perfusion imaging in nuclear cardiology. *Eur J Nucl Med Mol Imaging* 2005;32:855-97.
3. Strauss HW, Miller DD, Wittry MD, et al. Society of Nuclear Medicine Procedure Guideline for Myocardial Perfusion Imaging. 2002. http://interactive.snm.org/docs/pg_ch02_0403.pdf. Accessed 29 Aug 2009.
4. Machac J, Bacharach SL, Bateman TM, et al; Quality Assurance Committee of the American Society of Nuclear Cardiology. Positron emission tomography myocardial perfusion and glucose metabolism imaging. *J Nucl Cardiol* 2006;13:e121-51.
5. Goerres GW, Burger C, Kamel E, et al. Respiration-induced attenuation artifact at PET/CT: technical considerations. *Radiology* 2003;226:906-10.
6. Pan T, Mawlawi O, Luo D, et al. Attenuation correction of PET cardiac data with low-dose average CT in PET/CT. *Med Phys* 2006;33:3931-8.
7. Le Meunier L, Maass-Moreno R, Carrasquillo JA, et al. PET/CT imaging: effect of respiratory motion on apparent myocardial uptake. *J Nucl Cardiol* 2006;13:821-30.
8. Martinez-Möller A, Souvatzoglou M, Navab N, et al. Artifacts from misaligned CT in cardiac perfusion PET/CT studies: frequency, effects, and potential solutions. *J Nucl Med* 2007;48:188-93.
9. Alessio AM, Kohlmyer S, Branch K, et al. Cine CT for attenuation correction in cardiac PET/CT. *J Nucl Med* 2007;48:794-801.

10. Gould KL, Pan T, Loghin C, et al. Frequent diagnostic errors in cardiac PET/CT due to misregistration of CT attenuation and emission PET images: a definitive analysis of causes, consequences, and corrections. *J Nucl Med* 2007;48:1112-21.
11. Nye JA, Esteves F, Votaw JR. Minimizing artifacts resulting from respiratory and cardiac motion by optimization of the transmission scan in cardiac PET/CT. *Med Phys* 2007;34:1901-6.
12. Souvatzoglou M, Bengel F, Busch R, et al. Attenuation correction in cardiac PET/CT with three different CT protocols: a comparison with conventional PET. *Eur J Nucl Med Mol Imaging* 2007;34:1991-2000.
13. Lautamäki R, Brown TL, Merrill J, Bengel FM. CT-based attenuation correction in (82)Rb-myocardial perfusion PET-CT: incidence of misalignment and effect on regional tracer distribution. *Eur J Nucl Med Mol Imaging* 2008;35:305-10.
14. McQuaid SJ, Hutton BF. Sources of attenuation-correction artefacts in cardiac PET/CT and SPECT/CT. *Eur J Nucl Med Mol Imaging* 2008;35:1117-23.
15. Loghin C, Sdringola S, Gould KL. Common artifacts in PET myocardial perfusion images due to attenuation-emission misregistration: clinical significance, causes, and solutions. *J Nucl Med* 2004;45:1029-39.
16. Gould KL, Pan T, Loghin C, et al. Reducing radiation dose in rest-stress cardiac PET/CT by single post stress cine CT for attenuation correction: quantitative validation. *J Nucl Med* 2008;49:738-45.
17. Sdringola S, Nakagawa K, Nakagawa Y, et al. Combined intense lifestyle and pharmacologic lipid treatment further reduce coronary events and myocardial perfusion abnormalities compared with usual-care cholesterol-lowering drugs in coronary artery disease. *J Am Coll Cardiol* 2003;41:263-72.

18. Johnson NP, Gould KL. Clinical evaluation of a new concept: resting myocardial perfusion heterogeneity quantified by markovian analysis of PET identifies coronary microvascular dysfunction and early atherosclerosis in 1,034 subjects. *J Nucl Med* 2005;46:1427-37.
19. Sdringola S, Loghin C, Boccalandro F, Gould KL. Mechanisms of progression and regression of coronary artery disease by PET related to treatment intensity and clinical events at long-term follow-up. *J Nucl Med* 2006;47:59-67.
20. Gould KL, Ornish D, Scherwitz L, et al. Changes in myocardial perfusion abnormalities by positron emission tomography after long-term, intense risk factor modification. *JAMA* 1995;274:894-901.
21. Gould KL, Martucci JP, Goldberg DI, et al. Short-term cholesterol lowering decreases size and severity of perfusion abnormalities by positron emission tomography after dipyridamole in patients with coronary artery disease. A potential noninvasive marker of healing coronary endothelium. *Circulation* 1994;89:1530-8.
22. Gould KL. Assessing progression or regression of CAD: the role of perfusion imaging. *J Nucl Cardiol* 2005;12:625-38.
23. Yoshida K, Mullani N, Gould KL. Coronary flow and flow reserve by PET simplified for clinical applications using rubidium-82 or nitrogen-13-ammonia. *J Nucl Med* 1996;37:1701-12.

TABLES

Table 1. Quantitative [relative](#) defect endpoints comparing helical and software-shifted helical CT for N=93 paired studies demonstrating rest or stress artifacts.

Endpoint	Helical	Shifted helical	p
Whole heart average (%)	76.8 ± 4.7%	78.5 ± 4.0%	NS
Severity (minimum quadrant average, SD)	-3.5 ± 1.9 SD	-3.0 ± 1.6 SD	0.0020
Severity (maximum quadrant average, SD)	-0.7 ± 1.2 SD	-0.7 ± 1.2 SD	NS
Size (%≤2.0 SD)	29.3 ± 19.2%	22.1 ± 17.0%	<0.0001
Size (%≤2.5 SD)	20.3 ± 17.2%	14.0 ± 13.7%	<0.0001
Size-severity (%<60% maximum)	4.7 ± 9.5%	2.4 ± 4.2%	0.0028
Size-severity (%≥80% maximum)	38.7 ± 17.0%	44.4 ± 19.3%	0.0002

NS=not significant, SD=standard deviation

For Peer Review

Table 2. Quantitative defect endpoints comparing helical and software-shifted helical CT separating rest and stress artifacts for the 93 paired studies with misregistration artifacts.

Endpoint	Rest (N=66)			Stress (N=27)		
	Helical	Shifted helical	p	Helical	Shifted helical	p
Relative str/rst ratio ≤ 0.66 (%)	0.2 ± 0.1	0.9 ± 0.7	NS	0.2 ± 0.1	0.2 ± 0.1	NS
Relative str/rst ratio 0.67-1.0 (%)	35.0 ± 1.9	42.6 ± 2.2	0.0002	54.2 ± 3.3	47.6 ± 3.4	0.0167
Relative str/rst ratio > 1.0 (%)	64.8 ± 2.0	56.5 ± 2.3	0.0001	45.6 ± 3.3	52.2 ± 3.5	0.0173
Absolute str/rst ratio ≤ 0.9 (%)	0.5 ± 0.2	79.5 ± 4.9	<0.0001	0.8 ± 0.4	0.3 ± 0.2	NS
Absolute str/rst ratio 0.91-1.4 (%)	48.7 ± 4.4	15.1 ± 4.0	<0.0001	61.3 ± 7.3	24.5 ± 7.1	0.0001
Absolute str/rst ratio > 1.4 (%)	50.8 ± 4.5	5.5 ± 2.2	<0.0001	38.0 ± 7.4	75.2 ± 7.1	0.0001
Whole heart absolute uptake (100 μ Ci/cc)	361 ± 22	389 ± 23	0.0002	426 ± 43	451 ± 49	0.0075
Minimum quadrant average absolute uptake (100 μ Ci/cc)	349 ± 22	378 ± 22	0.0007	399 ± 37	429 ± 44	0.0119
Maximum quadrant average absolute uptake (100 μ Ci/cc)	394 ± 23	411 ± 25	0.0073	470 ± 51	483 ± 55	NS

NS=not significant, Str/rst=stress/rest, % = percent of left ventricle

*Absolute uptake only available for N=13 rest studies and N=8 stress studies.

Table 3. Quantitative relative defect endpoints comparing helical and cine CT for N=161 paired studies demonstrating rest or stress artifacts.

Endpoint	Helical	Cine	p
Whole heart average (%)	76.8 ± 0.4%	78.6 ± 0.3%	NS
Severity (minimum quadrant average, SD)	-3.6 ± 0.2 SD	-3.1 ± 0.2 SD	0.0001
Severity (maximum quadrant average, SD)	-0.7 ± 0.1 SD	-0.5 ± 0.1 SD	0.0002
Size (%≤2.0 SD)	28.9 ± 1.5%	20.9 ± 1.3%	<0.0001
Size (%≤2.5 SD)	20.2 ± 1.4%	13.8 ± 1.1%	<0.0001
Size-severity (%<60% maximum)	6.0 ± 0.8%	4.1 ± 0.6%	0.0003
Size-severity (%≥80% maximum)	40.5 ± 1.4%	47.3 ± 1.3%	<0.0001

NS=not significant, SD=standard deviation

Deleted: Table 3. Agreement on binary defect endpoints between helical and software-shifted helical CT¶

¶
Endpoint

Deleted: 4

For Peer Review

Table 4. Quantitative defect endpoints comparing helical and cine CT separating rest and stress artifacts for the 161 paired studies with misregistration artifacts.

Deleted: 5

Endpoint	Rest (N=101)			Stress (N=60)		
	Helical	Cine	p	Helical	Cine	p
Relative str/rst ratio ≤ 0.66 (%)	0.8 ± 0.3	0.4 ± 0.1	NS	1.1 ± 0.5	1.1 ± 0.6	NS
Relative str/rst ratio 0.67-1.0 (%)	38.9 ± 1.7	40.9 ± 1.7	NS	57.2 ± 2.1	53.2 ± 2.0	0.0096
Relative str/rst ratio > 1.0 (%)	60.3 ± 1.8	58.6 ± 1.7	NS	41.7 ± 2.2	45.7 ± 2.2	0.0100
Absolute str/rst ratio ≤ 0.9 (%)	1.9 ± 0.5	1.8 ± 0.5	NS	2.5 ± 0.9	1.9 ± 0.7	NS
Absolute str/rst ratio 0.91-1.4 (%)	56.8 ± 3.5	59.8 ± 3.6	0.0082	59.2 ± 4.7	59.1 ± 4.8	NS
Absolute str/rst ratio > 1.4 (%)	41.3 ± 3.6	38.4 ± 3.7	0.0116	38.3 ± 4.9	39.0 ± 5.0	NS
Whole heart absolute uptake (100 μ Ci/cc)	352 ± 11	367 ± 12	0.0001	487 ± 41	504 ± 40	0.0480
Minimum quadrant average absolute uptake (100 μ Ci/cc)	342 ± 12	353 ± 12	0.0017	462 ± 39	488 ± 39	0.0171
Maximum quadrant average absolute uptake (100 μ Ci/cc)	382 ± 12	394 ± 12	0.0011	523 ± 43	530 ± 42	NS

NS=not significant, Str/rst=stress/rest, % = percent of left ventricle.

*Absolute uptake only available for N=51 rest studies and N=16 stress studies.

Table 5. Quantitative endpoint differences from the optimal CT attenuation technique by various attenuation CT techniques

Endpoint	Δ Helical	p	Δ Shifted Helical	p	Δ Cine	P
Sample size (N)	177	N/A	93	N/A	161	N/A
Whole heart average (%)	3.6 (2.5-4.5)	<0.0001	2.9 (2.3-3.4)	0.0008	0.7 (0.4-0.8)	0.0428
Severity (minimum quadrant average, SD)	1.5 (0.8-1.9)	<0.0001	1.0 (0.8-1.2)	<0.0001	0.4 (0.1-0.6)	0.0203
Severity (maximum quadrant average, SD)	0.8 (0.6-0.9)	<0.0001	1.0 (0.8-1.2)	0.0173	0.3 (0.1-0.3)	NS
Size (%≤2.0 SD)	15.0 (12.2-17.4)	<0.0001	11.8 (8.9-14.0)	<0.0001	2.0 (1.3-2.5)	NS
Size (%≤2.5 SD)	13.2 (10.2-15.7)	<0.0001	9.3 (6.7-11.4)	<0.0001	1.6 (0.9-2.0)	0.0214
Size-severity (%<60% maximum)	7.5 (0.5-10.6)	0.0001	3.7 (0.0-5.3)	0.0035	0.7 (0.3-1.0)	0.0344
Size-severity (%≥80% maximum)	13.2 (11.2-15.0)	<0.0001	14.0 (11.6-16.1)	0.0047	3.1 (1.9-4.0)	NS
Relative str/rst ratio≤0.66 (%)	4.2 (0.0-6.5)	NS	0.7 (0.3-0.9)	NS	0.0 (0.0-0.1)	NS
Relative str/rst ratio 0.67-1.0 (%)	14.0 (12.0-15.8)	NS	16.2 (14.0-18.0)	NS	4.5 (2.9-5.7)	NS
Relative str/rst ratio>1.0 (%)	14.2 (12.2-15.9)	NS	16.9 (14.5-19.1)	NS	4.5 (2.9-5.7)	NS
Absolute str/rst ratio≤0.9 (%)	36.3 (22.5-46.1)	0.0045	51.9 (33.6-65.3)	<0.0001	22.2 (0.0-32.4)	NS
Absolute str/rst ratio 0.91-1.4 (%)	12.2 (7.2-15.6)	NS	57.1 (48.7-64.3)	<0.0001	1.7 (0.2-2.4)	NS
Absolute str/rst ratio>1.4 (%)	11.8 (6.7-15.2)	0.0007	55.3 (46.9-62.6)	0.0078	1.6 (0.0-2.3)	NS
*Whole heart absolute uptake (100*μCi/cc)	29.4 (23.2-34.5)	<0.0001	25.0 (10.5-33.8)	NS	9.1 (0.0-15.7)	NS
*Minimum quadrant average absolute uptake (100*μCi/cc)	30.9 (20.5-38.6)	<0.0001	24.7 (12.8-32.5)	NS	5.5 (0.0-9.6)	NS
*Maximum quadrant average absolute uptake (100*μCi/cc)	28.0 (21.8-33.1)	0.0003	28.7 (13.3-38.4)	NS	8.5 (0.0-14.7)	NS

Δ values are expressed as quadratic mean (95% confidence interval) and the p value arises from a paired t-test, Str/rst=stress/rest

*Absolute uptake Δ only available for N=67 paired helical comparisons, N=21 paired software-shifted helical comparisons, and N=67 paired cine comparisons.

Deleted: ¶

¶

¶

¶

Table 6. Agreement on binary defect endpoints between helical and cine CT¶

¶

Endpoint

...

Deleted: 7

FIGURE LEGENDS

Figure 1. Orientation of myocardial perfusion images displayed in four 90° views corresponding to coronary artery distributions as previously reported (17, 19-22).

Figure 2. Myocardial perfusion images by helical CT-PET with an artifactual defect (blue and green) due to misregistration of the CT image (white arrow) and the emission images (purple arrow) on CT-PET fusion images. Shifting the helical CT images to co-register properly with the emission images eliminates this false positive result. The color bar indicates the relative scale of activity from maximum in white through decreasing steps to red, yellow, green, blue and black for the lowest activity.

Figure 3. Artifactual defects on helical CT-PET at rest (green) due to misregistration (arrows) that improve but remain substantially abnormal after shifting CT data to achieve co-registration. This artifact resolves on resting and stress cine CT-PET where the CT data is acquired over two breath cycles such that the average CT attenuation correction during breathing matches the average attenuation during breathing of the emission data acquisition. The minimal heterogeneity of the resting cine CT-PET that improves with dipyridamole stress is common on people with risk factors for atherosclerosis as a potential marker of early atherosclerosis as previously reported (18).

Figure 4. Artifactual defects on cine CT-PET (green) due to the patient taking a "big sigh" during the cine CT acquisition resulting in a "gap" in attenuation correction seen in the fusion scan (white arrow). Removing the attenuation data during this "sigh" part of the breathing cycle and using the remaining breath cycles of the cine CT for reconstruction substantially reduces the artifact. The helical CT-PET does not show this gap since it is acquired as a brief "snapshot" during a shorter time interval of the breath cycle. The resting heterogeneity on both the corrected cine CT-PET and the helical CT-PET improves after dipyridamole stress with a small remaining stress defect in the distribution of a small anterior coronary artery branch and the distal Posterior Descending coronary artery (black arrows). The severe

resting perfusion heterogeneity that improves after dipyridamole stress is associated with coronary artery disease (18), likely due to endothelial dysfunction known to cause resting perfusion heterogeneity.

Figure 5. Artifactual defects (green and blue) caused by defibrillator leads in the right ventricle that show a high-density region or star pattern (arrow) on both helical or cine CT. This localized high density in the attenuation data over-corrects the inferior myocardium leaving severe relative anterior and lateral defects on rest and dipyridamole stress images. Repeat rest/stress dipyridamole PET using the Positron Corporation scanner with a rotating rod attenuation correction method eliminates this artifact to show a mild stress induced defect in the anterior septum due to mild LAD disease consistent with the coronary arteriogram.

For Peer Review

Page 22: [1] Deleted me 10/17/2009 3:21:00 PM

Table 3. Agreement on binary defect endpoints between helical and software-shifted helical CT

Endpoint		Shifted helical no	Shifted helical yes	
Minimum quadrant average > 2.0SD				$\kappa=0.34$
	Helical no	11	6	p via κ
	Helical yes	17	59	0.0003
Minimum quadrant average > 2.5SD				$\kappa=0.47$
	Helical no	22	6	p via κ
	Helical yes	17	48	<0.0001
>5% under 60% maximum				$\kappa=0.41$
	Helical no	69	3	p via κ
	Helical yes	13	8	<0.0001
>5% \leq 2.0 SD				$\kappa=0.14$
	Helical no	2	2	p via κ
	Helical yes	14	75	0.0378
>5% \leq 2.5 SD				$\kappa=0.50$
	Helical no	16	3	p via κ
	Helical yes	16	58	<0.0001

Page Break

Page 24: [2] Deleted me 10/17/2009 3:21:00 PM

Table 6. Agreement on binary defect endpoints between helical and cine CT

Endpoint		Cine no	Cine yes	
Minimum quadrant average > 2.0SD				$\kappa=0.50$
	Helical no	27	10	p via κ
	Helical yes	22	102	<0.0001
Minimum quadrant average > 2.5SD				$\kappa=0.54$
	Helical no	47	9	p via κ
	Helical yes	27	78	<0.0001
>5% under 60% maximum				$\kappa=0.64$
	Helical no	109	4	p via κ
	Helical yes	18	30	<0.0001
>5% \leq 2.0 SD				$\kappa=0.65$
	Helical no	13	1	p via κ
	Helical yes	11	136	<0.0001
>5% \leq 2.5 SD				$\kappa=0.51$
	Helical no	27	3	p via κ

	Helical yes	29	102	<0.0001
--	-------------	----	-----	---------

.....Page Break.....

For Peer Review

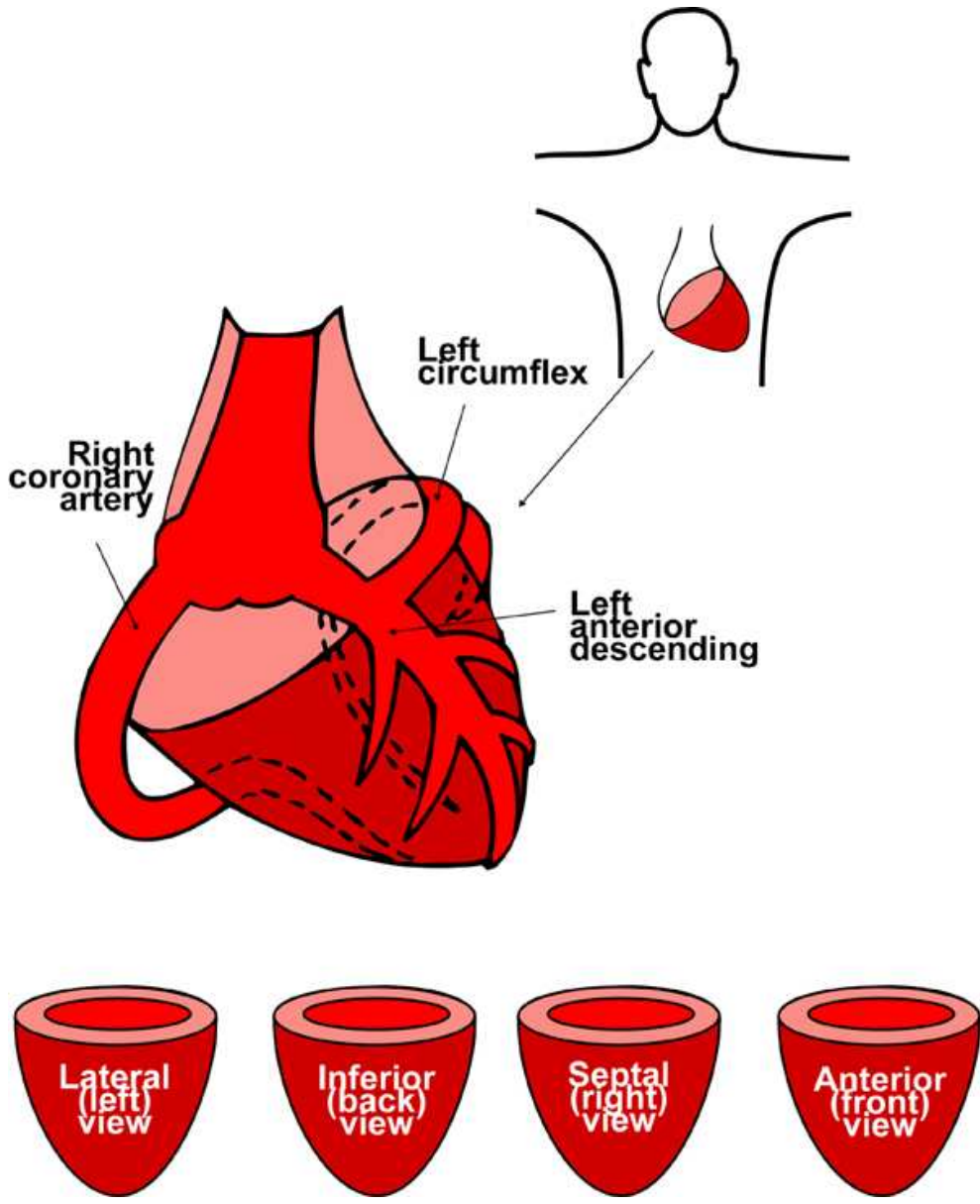


Figure 1. Orientation of myocardial perfusion images displayed in four 90° views corresponding to coronary artery distributions as previously reported (17, 19-22).
211x258mm (72 x 72 DPI)

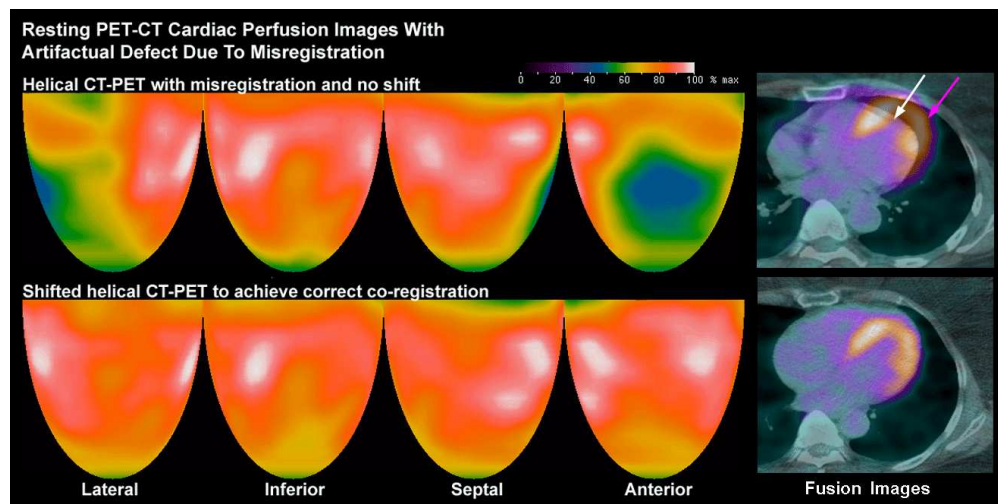


Figure 2. Myocardial perfusion images by helical CT-PET with an artifactual defect (blue and green) due to misregistration of the CT image (white arrow) and the emission images (purple arrow) on CT-PET fusion images. Shifting the helical CT images to co-register properly with the emission images eliminates this false positive result. The color bar indicates the relative scale of activity from maximum in white through decreasing steps to red, yellow, green, blue and black for the lowest activity.

465x233mm (72 x 72 DPI)

Review

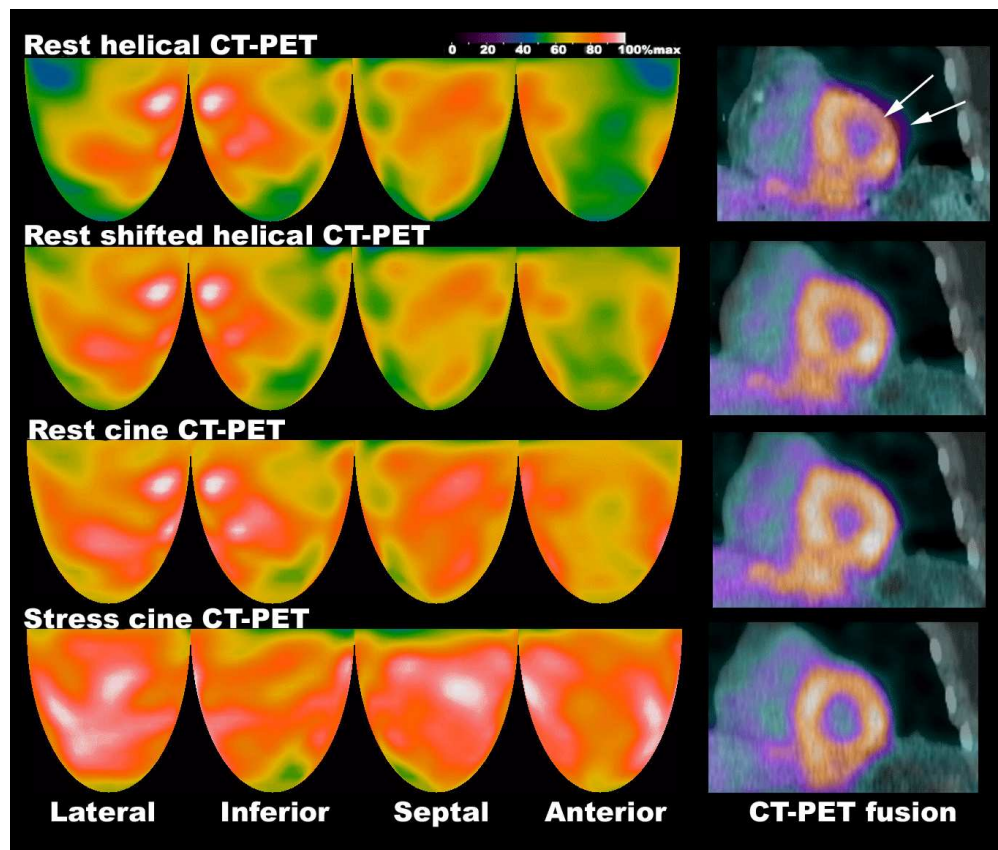


Figure 3. Artfactual defects on helical CT-PET at rest (green) due to misregistration (arrows) that improve but remain substantially abnormal after shifting CT data to achieve co-registration. This artifact resolves on resting and stress cine CT-PET where the CT data is acquired over two breath cycles such that the average CT attenuation correction during breathing matches the average attenuation during breathing of the emission data acquisition. The minimal heterogeneity of the resting cine CT-PET that improves with dipyridamole stress is common on people with risk factors for atherosclerosis as a potential marker of early atherosclerosis as previously reported (18).
481x407mm (72 x 72 DPI)

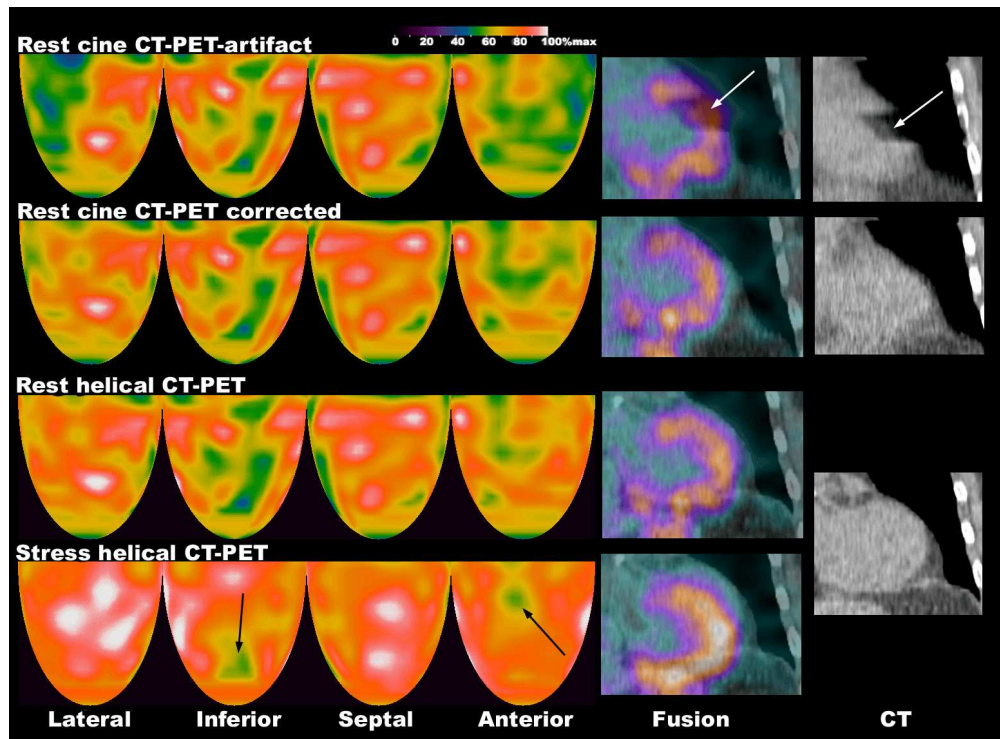


Figure 4. Artfactual defects on cine CT-PET (green) due to the patient taking a “big sigh” during the cine CT acquisition resulting in a “gap” in attenuation correction seen in the fusion scan (white arrow). Removing the attenuation data during this “sigh” part of the breathing cycle and using the remaining breath cycles of the cine CT for reconstruction substantially reduces the artifact. The helical CT-PET does not show this gap since it is acquired as a brief “snapshot” during a shorter time interval of the breath cycle. The resting heterogeneity on both the corrected cine CT-PET and the helical CT-PET improves after dipyridamole stress with a small remaining stress defect in the distribution of a small anterior coronary artery branch and the distal Posterior Descending coronary artery (black arrows). The severe resting perfusion heterogeneity that improves after dipyridamole stress is associated with coronary artery disease (18), likely due to endothelial dysfunction known to cause resting perfusion heterogeneity.

548x402mm (72 x 72 DPI)

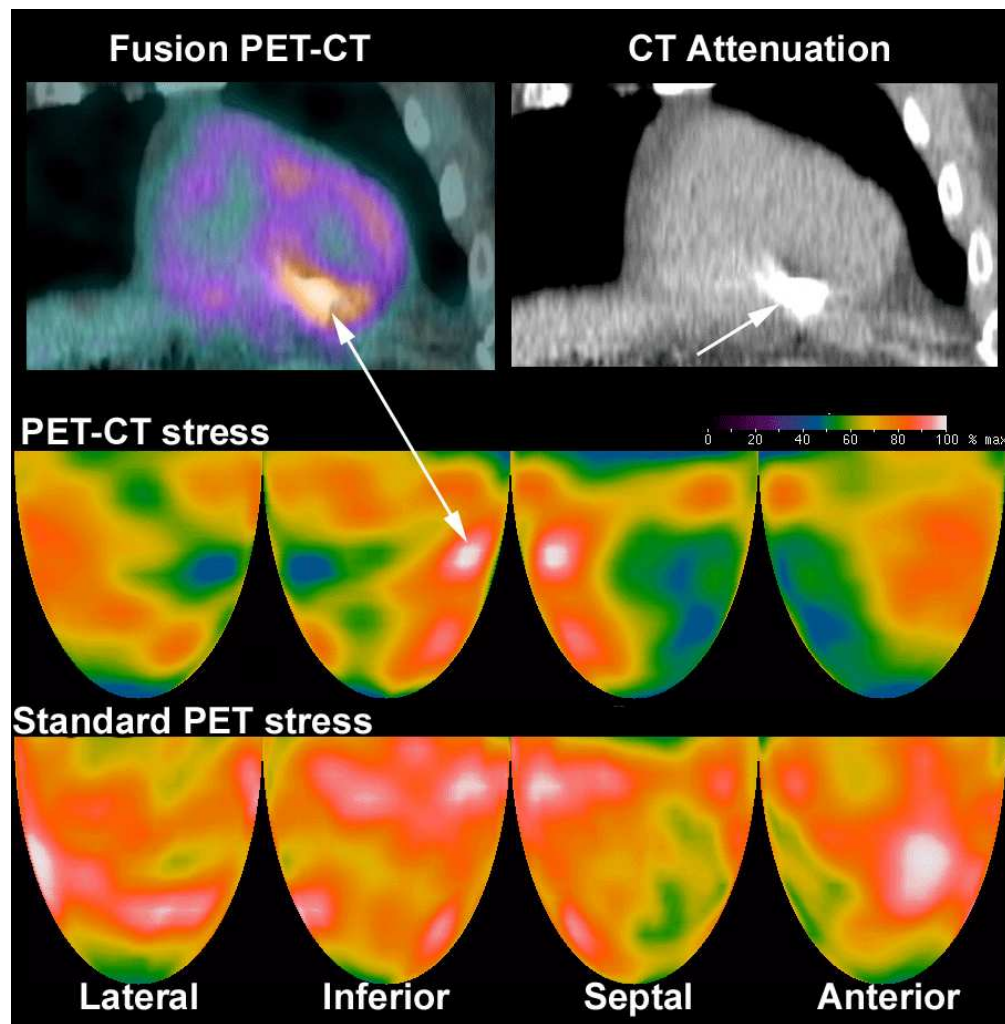


Figure 5. Artfactual defects (green and blue) caused by defibrillator leads in the right ventricle that show a high-density region or star pattern (arrow) on both helical or cine CT. This localized high density in the attenuation data over-corrects the inferior myocardium leaving severe relative anterior and lateral defects on rest and dipyridamole stress images. Repeat rest/stress dipyridamole PET using the Positron Corporation scanner with a rotating rod attenuation correction method eliminates this artifact to show a mild stress induced defect in the anterior septum due to mild LAD disease consistent with the coronary arteriogram.

318x324mm (72 x 72 DPI)